JOURNAL OF COMPUTATIONAL PHYSICS **144,** 460–483 (1998)
ARTICLE NO. CP985994

The Design of Local Navier–Stokes Preconditioning for Compressible Flow

Dohyung Lee

Department of Aerospace Engineering, University of Michigan, Ann Arbor, Michigan 48109-2118
E-mail: dohyung@engin.umich.edu

Received May 22, 1997; revised December 31, 1997

A family of Navier–Stokes preconditioners is presented that may reduce the stiffness due to complicated interaction between convection and diffusion in viscous flows. Navier–Stokes preconditioning is developed based on a Fourier analysis of the discretized equations and a dispersion analysis of the differential equations. Navier–Stokes preconditioning can be extended from the Euler technique with two methods: (a) by using block-Jacobi preconditioning for the viscous terms; (b) by introducing analytic dependence on the cell-Reynolds number in the preconditioner. With these techniques it is possible to produce a local Navier–Stokes preconditioner effective for all Mach and cell-Reynolds numbers. These techniques and a combined method are analyzed with respect to condition number and linear wave propagation and are illustrated with some numerical results.

1. INTRODUCTION

As discussed in the companion paper [9] on Euler preconditioning, the technique of marching the unsteady Euler and Navier–Stokes equations to a steady state is widely used for the computation of compressible flows. In the Euler equations, the stiffness of the time-dependent method is mainly decided by a *condition number*, which is the ratio of the largest to the smallest convective wave speed. The condition number increases without bound at low-speed and transonic flow. With the presence of viscous terms, the stiffness is decided by the complicated interaction of both propagating and damping effects. In this case, the stiffness of viscous compressible flow is indicated by a newly defined *condition number*, which is now the ratio of the largest to the smallest modulus of a complex wave speed; the complex wave speed contains the information about the scales of both the wave propagation and damping in the form of a complex variable. Using the modulus yields continuous switching between pure propagation and pure damping. Therefore, analogous to the inviscid case when the condition number approaches one, the Navier–Stokes system

0021-9991/98 $25.00

is well-conditioned and as the number increases, the system becomes stiff, resulting in convergence degradation.

As to local preconditioning for the Navier–Stokes equations, the research findings are more recent than the Euler results, and more limited in number. Venkateswaran *et al.* [15, 3] contributed a valuable method of analysis by which the proper dependence of the preconditioning on the Reynolds number can be determined. Godfrey *et al.* [8, 7, 6] circumvented the use of such an analysis by composing a Navier–Stokes preconditioner from the optimal Euler preconditioner and the Jacobi block for the discretized viscous/conductive terms.

Allmaras [2], and Pierce and Giles [12] considered pure block-Jacobi preconditioning for the discretized Navier–Stokes equations, equivalent to using block-Jacobi relaxation. This type of preconditioning always provides good high-frequency damping, which is desirable for multigrid relaxation, but does not systematically reduce the condition number, nor does it help preserve accuracy in the low-speed Euler limit.

The object of this paper is to present various forms of Navier–Stokes preconditioners, based on the Fourier analysis of the discretized equations and a dispersion analysis of the differential equations. To design Navier–Stokes preconditioning, it is necessary to use both dispersion analysis and Fourier footprint analysis for discretized spatial operators. The dispersion analysis introduces the above condition number based on complex frequency. This tool is not sufficient because the footprint-scaling technique reveals the properties of all-frequency numerical waves, which cannot be analyzed by dispersion analysis, and it actually helps to filter out those preconditioners that produce dislocated high-frequency clusters.

The discrete Fourier analysis suggests a "Jacobi-type" Navier–Stokes preconditioner, combining an optimal Euler preconditioner with the Jacobi block for the discretized viscous/conductive terms. The dispersion analysis produces an analytical form of the preconditioner, which can equalize, in absolute value, the complex wave speeds of the Navier–Stokes equations. Both preconditioners and their combined form are analyzed with respect to condition number and linear wave propagation and are illustrated with numerical results.

2. ANALYSIS OF THE NAVIER–STOKES EQUATIONS

For the design of Navier–Stokes preconditioners the system of linearized equations is considered. In two dimensions these can be written as

$$\mathbf{U}_t = \mathbf{A}\mathbf{U}_x + \mathbf{B}\mathbf{U}_y + \mathbf{C}\mathbf{U}_{xx} + \mathbf{D}\mathbf{U}_{xy} + \mathbf{E}\mathbf{U}_{yy}. \tag{1}$$

The first two terms on the right-hand side are the spatial Euler operator; the remaining terms are viscous/conductive. In the discrete version the latter are approximated by central differencing. With the *parabolic symmetrizing set of variables* [1],

$$d\mathbf{U} = \begin{pmatrix} \frac{ad\rho}{\sqrt{\gamma}\rho} \\ du \\ dv \\ \frac{adT}{\sqrt{\gamma(\gamma-1)}T} \end{pmatrix}, \tag{2}$$

all convection and diffusion matrix coefficients become symmetric; if we choose x to be the streamwise coordinate, the matrices become particularly sparse:

$$\mathbf{A} = a\begin{pmatrix} M & \frac{1}{\sqrt{\gamma}} & 0 & 0 \\ \frac{1}{\sqrt{\gamma}} & M & 0 & \sqrt{\frac{\gamma-1}{\gamma}} \\ 0 & 0 & M & 0 \\ 0 & \sqrt{\frac{\gamma-1}{\gamma}} & 0 & M \end{pmatrix}, \qquad \mathbf{B} = a\begin{pmatrix} 0 & 0 & \frac{1}{\sqrt{\gamma}} & 0 \\ 0 & 0 & 0 & 0 \\ \frac{1}{\sqrt{\gamma}} & 0 & 0 & \sqrt{\frac{\gamma-1}{\gamma}} \\ 0 & 0 & \sqrt{\frac{\gamma-1}{\gamma}} & 0 \end{pmatrix}. \quad (3)$$

$$\mathbf{C} = \nu\begin{pmatrix} 0 & 0 & 0 & 0 \\ 0 & \frac{4}{3} & 0 & 0 \\ 0 & 0 & 1 & 0 \\ 0 & 0 & 0 & \frac{\gamma}{\mathrm{Pr}} \end{pmatrix}, \qquad \mathbf{D} = \nu\begin{pmatrix} 0 & 0 & 0 & 0 \\ 0 & 0 & \frac{1}{3} & 0 \\ 0 & \frac{1}{3} & 0 & 0 \\ 0 & 0 & 0 & 0 \end{pmatrix}, \qquad \mathbf{E} = \nu\begin{pmatrix} 0 & 0 & 0 & 0 \\ 0 & 1 & 0 & 0 \\ 0 & 0 & \frac{4}{3} & 0 \\ 0 & 0 & 0 & \frac{\gamma}{\mathrm{Pr}} \end{pmatrix}. \quad (4)$$

The physical characteristics of the Navier–Stokes equations over a broad range of the Reynolds numbers can be understood by performing a Fourier or dispersion analysis of the p.d.e.'s, and by examining Fourier footprints of a discretized spatial operators. While the p.d.e. analysis tells us only about the long waves (low frequencies) which behave according to the real physics, the Fourier footprint analysis provides the behavior of all modes produced by numerical discretization.

Venkateswaran *et al.* [15] performed dispersion analysis for 1D Navier–Stokes equations with the assumption of the unit Prandtl number and isotropic viscosity; in this case the equations decouple and distinct roots for complex wave speeds are obtained. By this analysis, there are three regimes in which the characteristics of solutions differ: (1) In the Euler limit, all modes are propagating without damping. (2) In the acoustic-dominant viscous case, even with very low cell-Reynolds number, two acoustic modes are propagating while one mode is damping. In this case, the order of the Mach number is much lower than that of the cell-Reynolds number. (3) When the cell-Reynolds number is low but the Mach number is not too low, i.e., the viscosity-dominant case, there are two modes damped due to the viscosity and heat conduction effect in momentum and energy equations whereas one mode is still propagating because of the non-viscous continuity equation.

Fourier analysis with a first order upwind scheme supports the results of dispersion analysis. In the Euler limit the Fourier footprint has three components: 2 larger half circles (size $\sim u \pm a_s$) for the acoustic modes and a small half circle (size $\sim u$) for entropy convection. Figures 1(a) and 1(b) show that when the acoustic Reynolds number ($Re_a = Re/M$) is large, the acoustic waves are dominant regardless of the cell-Reynolds number. Figures 1(c) and 1(d) demonstrate that when Re_a is small, two modes are viscous-dominant as Re decreases; the remaining mode does not experience a strong viscous effect. With low Re_a, the overall shape of the footprints becomes flatter as Re decreases, deviating significantly from the circular shape of the Euler footprints. The extent of the footprint along the negative real axis is inversely proportional to the cell-Reynolds number, which is the scale factor of the viscous Jacobian matrices. It is also noted that one or two components of the footprints get close to the imaginary axis while the others collapse onto the negative-real axis. These results can be interpreted in the same manner as those of the dispersion analysis: one or two

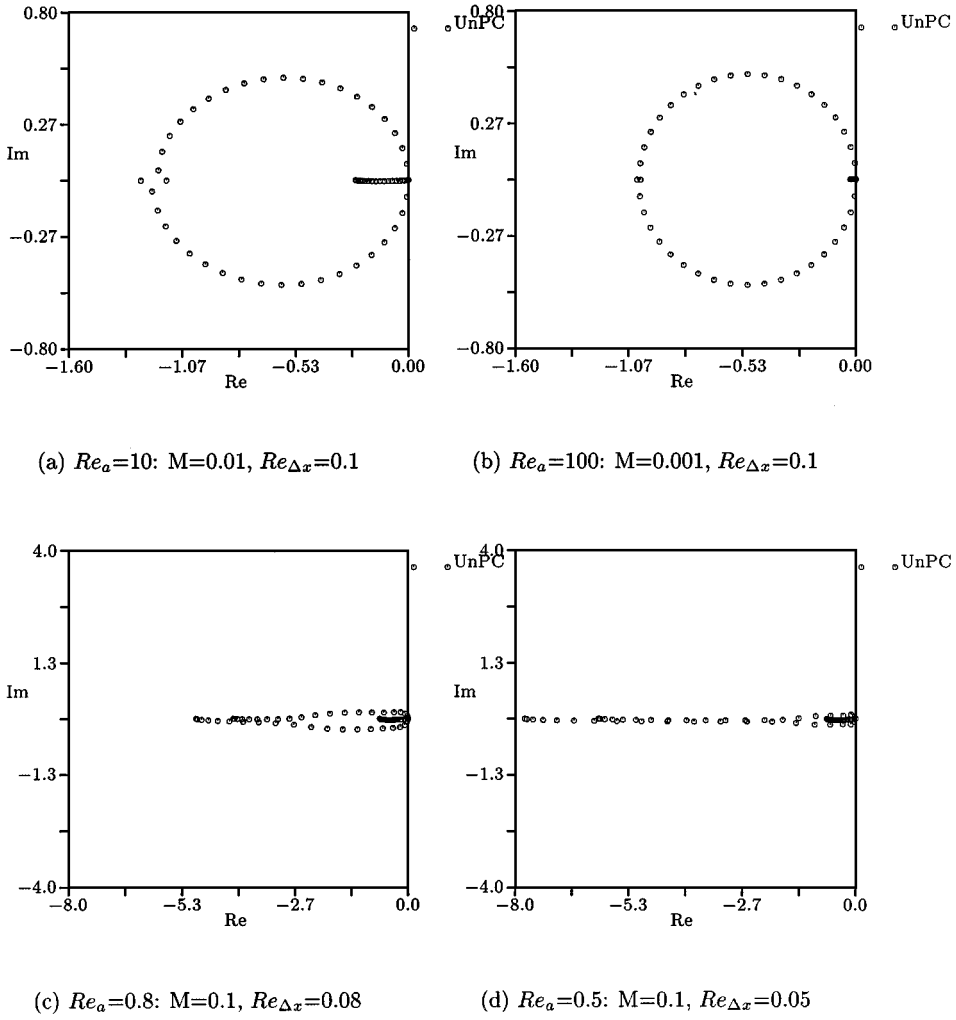

(a) Re_a=10: M=0.01, $Re_{\Delta x}$=0.1

(b) Re_a=100: M=0.001, $Re_{\Delta x}$=0.1

(c) Re_a=0.8: M=0.1, $Re_{\Delta x}$=0.08

(d) Re_a=0.5: M=0.1, $Re_{\Delta x}$=0.05

FIG. 1. Fourier footprint for the 1D N-S equations.

modes are still convection-dominated depending on the acoustic Reynolds number, while the other modes are viscosity dominated.

In designing Navier–Stokes preconditioning, both dispersion analysis and Fourier footprint analysis for discretized spatial operators are important. The first tool requires introducing a condition number based on the complex frequency, which includes both the wave speed and the damping rate; it is this condition number that must be optimized, as done for the wave-speed condition number in Euler preconditioning. The first tool is not sufficient because the footprint-scaling technique can show the characteristics of high-frequency numerical waves, which cannot be analyzed by dispersion analysis, and it actually helps to filter out those preconditioners that produce dislocated high-frequency clusters.

3. PRECONDITIONING DESIGN FOR NAVIER–STOKES EQUATIONS

Two ways of extending local Euler preconditioners to the Navier–Stokes equations have been reported in the literature:

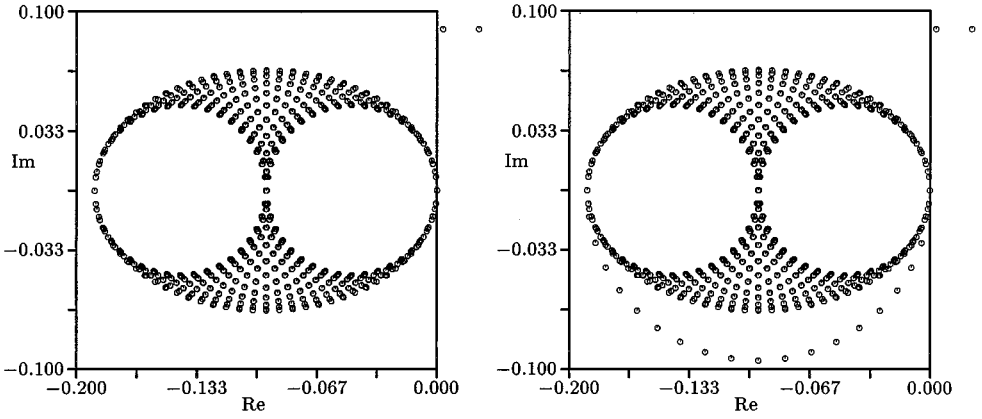

(a) M=0.1, Original preconditioning (b) M=0.1, Modified preconditioning

FIG. 2. Fourier footprints for the upwind-differenced 2D Euler equations with optimal preconditioning. In (a) the entropy/shear eigenvalues coincide with acoustic eigenvalues along the circular "hole" touching the origin; in (b) they have been rescaled and become visible.

(1) Adding to the Euler preconditioner the viscous/conductive entries arising in block-Jacobi preconditioning; this technique is due to Godfrey [6, 8, 7];

(2) Introducing the cell-Reynolds number dependence in the entries of the Euler preconditioner according to a Navier–Stokes dispersion analysis, a technique due to Venkateswaran *et al.* [15].

Jacobi Preconditioning

With regard to the first technique, the objections to Jacobi-type preconditioning for the Euler residual are not valid for the Navier–Stokes terms, because these terms by themselves are very well conditioned.[1] The main effect of Jacobi preconditioning when used only for the viscous/conductive terms is rescaling the dissipative scales with respect to the convection scales [10]. This is achieved in practice by fixing the highest-frequency eigenvalues (represented in the Fourier footprint by the left-most negative-real point), regardless of Mach or cell-Reynolds number.

However, the application of this technique to the 2D Navier–Stokes preconditioner requires some modification of the embedded Euler preconditioning. The Euler preconditioning, which is the basis for the Navier–Stokes preconditioning extension, is well discussed in the joint paper [9]. A Fourier footprint for the preconditioned 2D first-order upwind Euler operator is drawn in Fig. 2(a). For the original p.d.e.-based preconditioning, the high acoustic frequencies are located at the far left, whereas the high frequency components of enthalpy and entropy are in the middle of the domain. It is desirable to put the highest frequencies for all physical modes at the same location, for instance, to facilitate high-frequency damping by marching schemes, or residual smoothing. This relocation can be accomplished by scaling the enthalpy- and entropy-wave speeds by a factor $\tau(1 + \frac{AR}{\beta})$; this is accomplished in the Van Leer–Lee–Roe matrix [11, 10] by replacing the constraints 1 in the elements (2, 2)

[1] The dissipative time-scales do not differ more than a factor $\max(\gamma/Pr, 4/3)$.

and (4, 4) of the preconditioning matrix by the required factor ϵ. For this preconditioning matrix, the Euler symmetrizing system of variables, $d\mathbf{U} = (\frac{dp}{\rho a}, du, dv, dp - a^2 d\rho)^T$, is used,

$$\mathbf{P}_{\text{Eu}} = \begin{pmatrix} \frac{\tau}{\beta^2}M^2 & -\frac{\tau}{\beta^2}M & 0 & 0 \\ -\frac{\tau}{\beta^2}M & \frac{\tau}{\beta^2}+\epsilon & 0 & 0 \\ 0 & 0 & \tau & 0 \\ 0 & 0 & 0 & \epsilon \end{pmatrix}, \tag{5}$$

where $\beta = \sqrt{|1 - M^2|}$ and $\tau = \min(\beta, \beta/M) = \sqrt{1 - \min(M^2, M^{-2})}$. The Fourier footprint after this modification is shown in Fig. 2(b).

The resulting form of a Jacobi Navier–Stokes preconditioner in the streamwise coordinate becomes

$$\mathbf{P}_{\text{NS}}^{-1} = \mathbf{P}_{\text{Eu}}^{-1} + \frac{2}{\alpha}\left(\frac{\mathbf{C}}{\Delta x^2} + \frac{\mathbf{E}}{\Delta y^2}\right), \qquad \alpha = \frac{q(\beta + \mathcal{AR})}{\Delta x}, \mathcal{AR} = \frac{\Delta x}{\Delta y}; \tag{6}$$

here q is the flow speed. Note that in subsonic case τ becomes β. This formula is valid for first-order upwind differencing of the Euler terms; for a higher-order Euler discretizations like a κ-scheme, a correction factor $1 - \kappa$ to the Euler contribution is required [10],

$$\mathbf{P}_{\text{NS}}^{-1} = \mathbf{P}_{\text{Eu}}^{-1} + \frac{2}{\alpha(1-\kappa)}\left(\frac{\mathbf{C}}{\Delta x^2} + \frac{\mathbf{E}}{\Delta y^2}\right). \tag{7}$$

Figures 3–5 show how Jacobi preconditioning can confine the numerical eigenvalues regardless of Reynolds number, cell aspect-ratio, and higher order scheme.

In the Cartesian coordinate, i.e., when the flow direction is not aligned with grid orientation, the expression of the Navier–Stokes preconditioner needs some transformation of viscous matrix coefficients because spatial discretization is performed with respect to grid direction.

$$\mathbf{P}_{\text{NS}}^{-1} = \mathbf{P}_{\text{Eu}}^{-1} + \frac{2}{\alpha_q}\left(\frac{\mathbf{C}\,|\cos\phi| + \mathbf{E}\,|\sin\phi|}{\Delta x^2} + \frac{\mathbf{C}\,|\sin\phi| + \mathbf{E}\,|\cos\phi|}{\Delta y^2}\right). \tag{8}$$

Note that the above expression is defined still on the streamwise coordinate and the viscous part may be further simplified with some assumptions. The enthalpy/entropy scale factor ϵ in the Euler preconditioner is taken to be $(\beta + \mathcal{AR}_q)$ due to the streamwise cell aspect-ratio. The streamwise cell aspect-ratio is defined $\mathcal{AR}_q$ (see Fig. 6) as

$$\mathcal{AR}_q = \frac{\Delta S_x}{\Delta S_y} = \frac{|\sin\phi| + \mathcal{AR}\,|\cos\phi|}{|\cos\phi| + \mathcal{AR}\,|\sin\phi|}, \tag{9}$$

where ϕ is the flow angle with respect to grid orientation. Therefore, the highest frequency eigenvalues are located on the real axis at $-2\alpha_q$ with

$$\alpha_q = \frac{q}{\Delta x}(\beta + \mathcal{AR}_q), \tag{10}$$

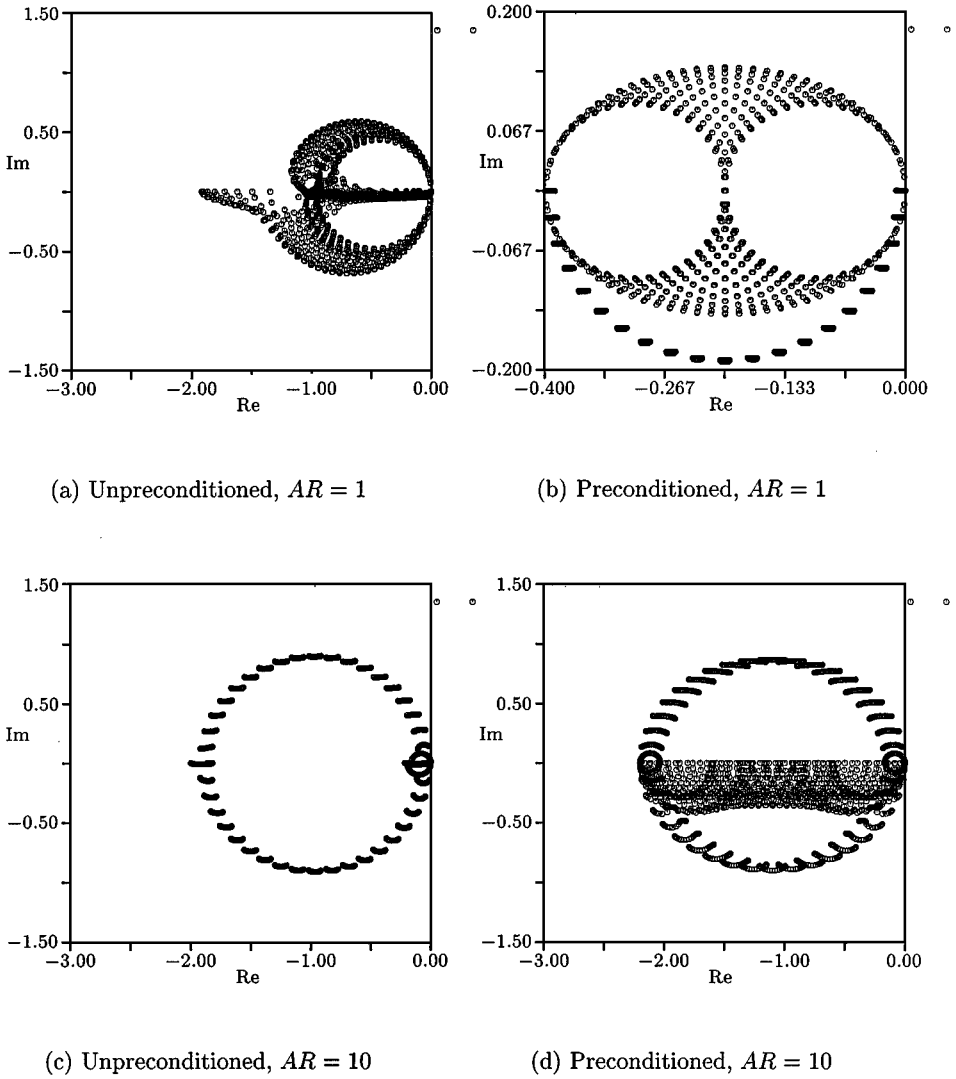

(a) Unpreconditioned, $AR = 1$ (b) Preconditioned, $AR = 1$

(c) Unpreconditioned, $AR = 10$ (d) Preconditioned, $AR = 10$

FIG. 3. Fourier footprint of Navier–Stokes spatial operator with or without preconditioning; $M = 0.1$, $Re_{\Delta x} = 10^2$.

for all Mach numbers and Reynolds numbers. However, this streamwise cell-aspect ratio concept can be applied to find the correct length scale in the definition of the local CFL number. The length scale for a general rectangular grid is defined as

$$l = \Delta S_x = \Delta X\,|\cos\phi| + \Delta Y\,|\sin\phi|. \tag{11}$$

The idea of rescaling through preconditioning can easily be extended to include source-term rescaling, and is in essence the same as the point-implicit treatment favored for a stiff source terms. This makes Jacobi-type Navier–Stokes preconditioning suitable for p.d.e.-based turbulence modeling and Navier–Stokes equations with finite-rate chemistry, which require the capacity to deal with stiff source terms as well as large cell-aspect ratios. If the source-term vector on the right-hand side is **H**, the preconditioner for the extended system

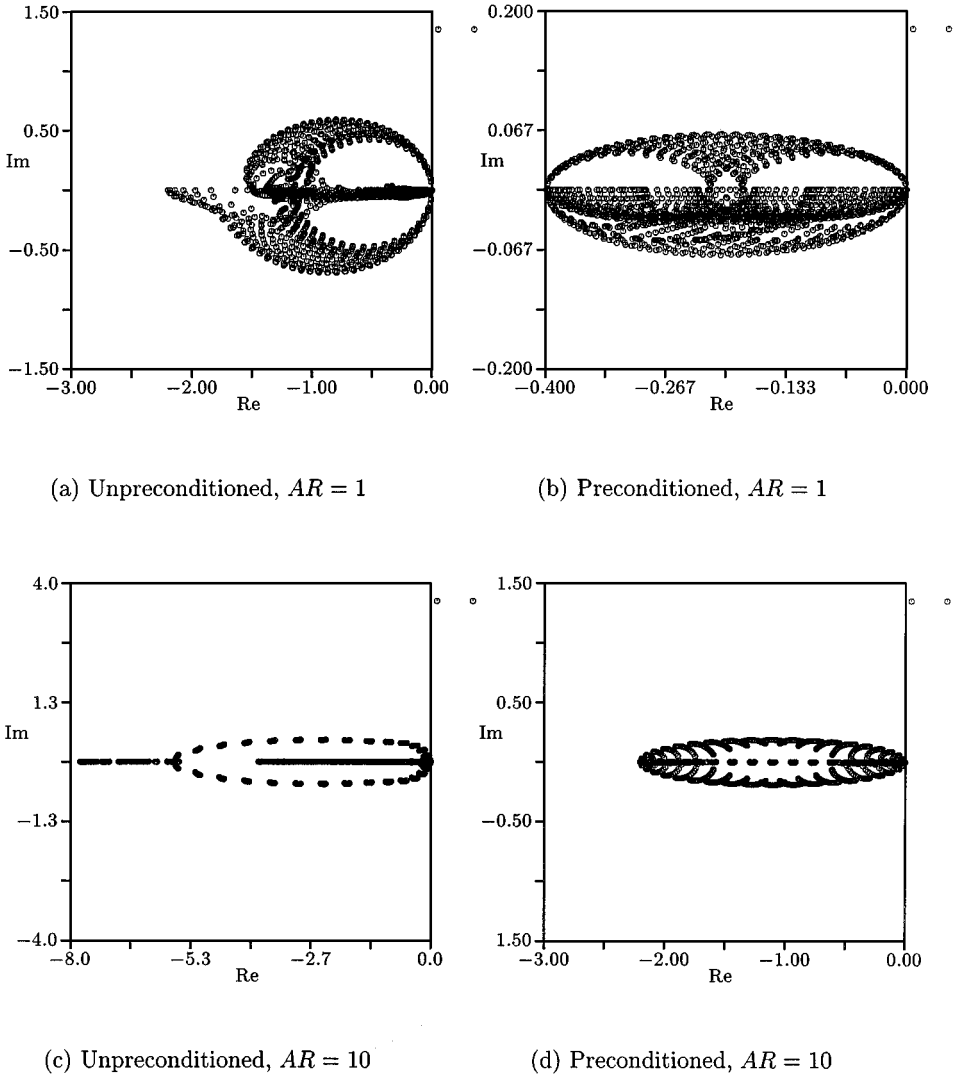

(a) Unpreconditioned, $AR = 1$

(b) Preconditioned, $AR = 1$

(c) Unpreconditioned, $AR = 10$

(d) Preconditioned, $AR = 10$

FIG. 4. Fourier footprint of Navier–Stokes spatial operator with or without preconditioning; $M = 0.1$, $Re_{\Delta x} = 1$.

of equations takes the form

$$\mathbf{P}_{\mathrm{NS,turb}}^{-1} = \mathbf{P}_{\mathrm{Eu}}^{-1} + \frac{1}{\alpha}\left(\frac{2\mathbf{C}}{\Delta x^2} + \frac{2\mathbf{E}}{\Delta y^2} - \Delta t \frac{\partial \mathbf{H}}{\partial \mathbf{U}}\right). \tag{12}$$

Figures 11 and 12 show how the Fourier footprint for this type of system is affected by the preconditioner. In Fig. 11 (unpreconditioned) notice that some eigenvalues, due to the presence of the source terms, have moved to a point on the negative real axis outside the main locus; this reduces the allowable time step. In Fig. 12 (preconditioned) these values have been scaled back.

Unlike Euler preconditioners, composite Navier–Stokes preconditioners of the above type are simplest when appearing as $\mathbf{P}^{-1}$. Analytical inversion is not attractive, so the method becomes truly point-implicit.

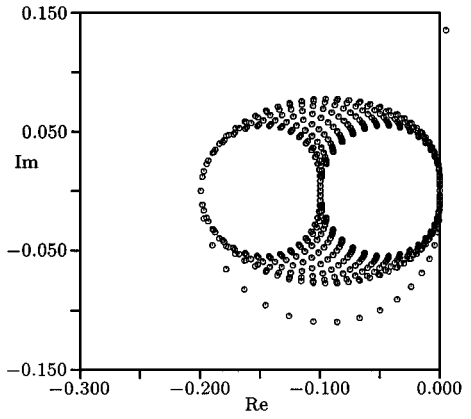

(a) Second-order ($\kappa = -1$), $M = 0.1$, $Re_x = 10^6$ (essentially inviscid case).

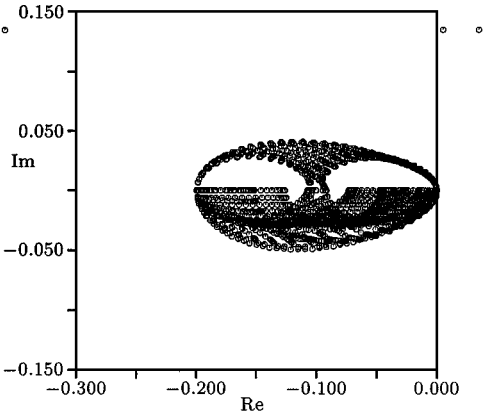

(b) Second-order ($\kappa = -1$), $M = 0.1$, $Re_x = 1$

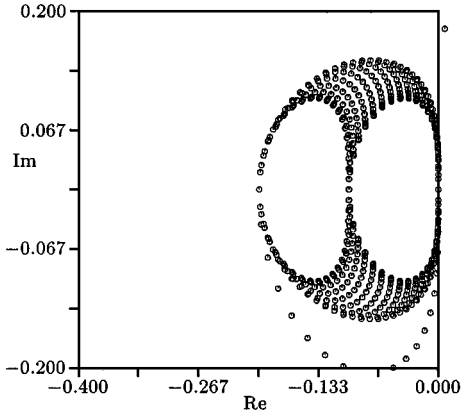

(c) Third-order ($\kappa = 1/3$), $M = 0.1$, $Re_x = 10^6$ (essentially inviscid case).

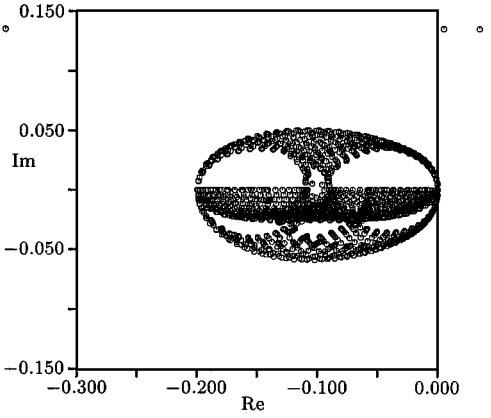

(d) Third-order ($\kappa = 1/3$), $M = 0.1$, $Re_x = 1$

FIG. 5. Fourier footprint of preconditioned Navier–Stokes spatial operator including higher-order upwind Euler operator.

Analytical Preconditioning

The analytical preconditioning requires a Fourier analysis of the linearized equation and subsequent eigenvalue computation as be shown in the previous section. In spite of symbolic computing, complete results have been obtained only for the unpreconditioned equations in one dimension, under simplifying assumptions. The effect of preconditioning can only be predicted in certain asymptotic cases (M and/or Re large or small); evaluating the performance of a proposed preconditioner requires numerical calculation of eigenvalues.

The eigenvalues coming out of a Navier–Stokes dispersion analysis are complex, with the imaginary part representing propagation and the negative real part damping. The condition

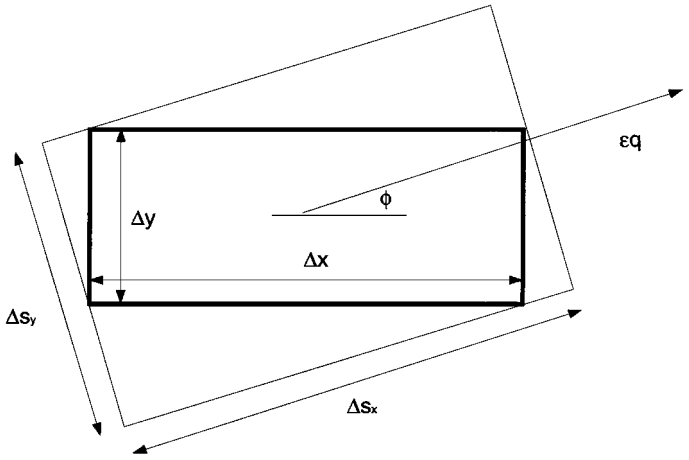

FIG. 6. Streamwise cell-aspect ratio ($\mathcal{AR}_q$). $\mathcal{AR}_q = \frac{\Delta S_x}{\Delta S_y}$, and $\mathcal{AR} = \frac{\Delta X}{\Delta Y}$. $\Delta S_x = \Delta X\,|\cos\phi| + \Delta Y\,|\sin\phi|$ and $\Delta S_y = \Delta X\,|\sin\phi| + \Delta Y\,|\cos\phi|$.

number still is defined as the ratio of the largest and smallest moduli of eigenvalues, and properly takes into account both physical effects. We therefore continue to pursue the optimization of the condition number. Using educated guessing and symbolic manipulation we have developed a family of 1D Navier–Stokes preconditioners that is capable of connecting the Van Leer–Lee–Roe Euler preconditioner to each of the two distinct asymptotic viscous regimes described below. Using the symmetrizing state variables listed earlier[2] we can write this matrix family as

$$\mathbf{P}_{\mathrm{VL,Analytic}} = \begin{pmatrix} P_{11} & -MQ & \frac{M^2Q-P_{11}}{\rho a} \\ -MQ & Q+1 & 0 \\ 0 & 0 & 1 \end{pmatrix}, \tag{13}$$

where P_{11} and Q must have the following asymptotic values: [15]:

$$P_{11} \sim \begin{cases} \mathcal{O}(M^2), & Re \gg 1 \\ \mathcal{O}\left(\frac{M^2}{Re^2}\right), & Re \ll 1,\ \frac{M^2}{Re} \ll 1,\ Q \sim \mathcal{O}(1). \\ \mathcal{O}\left(\frac{1}{Re}\right), & Re \ll 1,\ \frac{M^2}{Re} \gg 1 \end{cases} \tag{14}$$

The three asymptotic regimes are, respectively, the inviscid or Euler limit, the acoustic-dominated viscous limit, and the viscosity-dominated limit. When P_{11} follows the above orders, the condition number can remain at the order of 1, which is independent of M and Re (see Table I).

It should be mentioned that the Reynolds number used in the dispersion analysis is always based on the wave length of the Fourier mode considered. When using the results of this

[2] The symmetrizing variables defined previously by $d\mathbf{U} = (dp/\rho a, du, dv, dw, dS)$ are sometimes called the "Euler symmetrizing variables," and actually are not the best choice for a Navier–Stokes analysis. The "parabolic symmetrizing variables," with $d\mathbf{U} = (ad\rho/\sqrt{\gamma}\rho, du, dv, dw, adT/\sqrt{\gamma(\gamma-1)T})$, symmetrize *all* coefficient matrices in the Navier–Stokes equations [1].

TABLE I
Condition Number Produced by Various 1D Navier–Stokes Preconditioners in Different Asymptotic Regimes, Based on PDE Dispersion Analysis

Preconditioning	Inviscid	Viscosity-dominated	Acoustic dominated
None	$\frac{M+1}{\min(M,\lvert 1-M\rvert)}$	$\frac{\gamma}{Re}$	$\frac{M+1}{M}Re$
Chorin/Euler	$\mathcal{O}(1)$	$\frac{1}{Re^2}$	$\frac{1}{Re^2}$
Van Leer/Euler	1	$\frac{1}{M^2Re^2}$	$\frac{1}{Re^2}$
Turkel/Euler	1	$\frac{1}{M^2Re^2}$	$\frac{1}{Re^2}$
Van Leer + Jacobi	1	$< \frac{1}{M^2Re^2}$	$< \frac{1}{Re^2}$
Van Leer/*Re* + Jacobi	1	$\mathcal{O}(1)$	$\ll \frac{1}{Re^2}$
Van Leer/*Re*	1	$\mathcal{O}(1)$	$\mathcal{O}(1)$

Note. For a description of regimes and preconditioners see the main text. "Van Leer/*Re*" means Van Leer–Lee–Roe preconditioner with *Re*-dependent (1, 1) element. The notation "< ..." means "lower than ...; analytic form hard to obtain."

analysis for the formulation of a *Re*-dependent preconditioner, *Re* must be interpreted as the cell-Reynolds number Re_h.

Inserting $Q = 0$ produces the equivalent of Chorin's[3] preconditioner, used initially by Turkel [13] and preferably by Merkle *et al.* [4].

One problem with this preconditioner is that, according to the PDE analysis, it creates a small positive growth rate for one wave mode [15]. In practice this mode may be suppressed by the artificial dissipation present in the discretization, in particular if the marching scheme is implicit. This, of course, does not relieve us of the duty to search for better explicit preconditioners. It is conceivable that a smarter choice of the matrix elements will eventually remove the growing mode, and that the analysis can be extended to multidimensional preconditioning.

For multidimensional preconditioning, it becomes much harder to maintain the condition number independent of *M* and *Re* because waves propagate omnidirectionally with different convection speeds and damping rates and the analysis becomes complicated in combining the convection and damping. However, if we attempt to reduce the condition number in both *x* and *y* directions, Chorin's preconditioner might be the proper choice. This does not imply that Chorin's is unique as a proper choice of a multidimensional preconditioner because maintaining the condition number in two directions might not be necessary design criterion as shown in Euler preconditioning [11, 10]; in Euler preconditioning the maximum value among each wave speed in all directions, not all wave speeds for all directions, is counted to reduce the condition number.

Combined Preconditioning

When combining the previous Jacobi and analytic preconditioning, some problems of each preconditioner could be eliminated. The growing mode of the analytic preconditioner can be removed by combining the result of the dispersion analysis with the addition of the viscous Jacobi block. Some condition numbers produced by Jacobi preconditioning, which becomes large for a very low cell-Reynolds number, can be also much reduced.

[3] Named after Chorin because it relates to his artificial-compressibility method [5].

Specifically, we have modified the (1, 1) element in the Van Leer–Lee–Roe preconditioner (cf. Eq. (5)) according to the branched expression of Eq. (14), and then added the viscous Jacobi block, as in Eq. (6). The 2D form adopted is

$$\mathbf{P}^{-1}_{\mathrm{VLR}/Re/\mathrm{Jacobi}} = \mathbf{P}^{-1}_{VLR/Re} + \frac{2}{\alpha_{Re}}\left(\frac{\mathbf{C}}{\Delta x^2} + \frac{\mathbf{E}}{\Delta y^2}\right), \tag{15}$$

with

$$\mathbf{P}_{\mathrm{VLR}/Re} = \begin{pmatrix} \frac{\tau}{\beta^2}\sigma & -\frac{\tau}{\beta^2}M & 0 & 0 \\ -\frac{\tau}{\beta^2}M & \frac{\tau}{\beta^2}+1 & 0 & 0 \\ 0 & 0 & \tau & 0 \\ 0 & 0 & 0 & 1 \end{pmatrix}, \tag{16}$$

where

$$\sigma = \begin{cases} M^2, & Re \gg 1 \\ \frac{M^2}{Re^2}, & Re \ll 1,\ \frac{M^2}{Re} \ll 1 \\ \frac{1}{Re}, & Re \ll 1,\ \frac{M^2}{Re} \gg 1. \end{cases} \tag{17}$$

The parameter α_{Re}, which reflects the ratio of convection to the diffusion effect, must be redefined because of the change of the eigenvalue system of the *Re*-modified Euler preconditioner. The exact symbolic form of the eigenvalues of this modified Euler preconditioner is too complicated to obtain, but the acoustic eigenvalues approximately become $\sqrt{2\sigma}$ and M. Therefore, α_{Re} is redefined as $\frac{\sqrt{2\sigma}}{\Delta x}$ instead of $\frac{M\tau}{\Delta x}(1+\frac{\mathcal{AR}}{\beta})$.

Unlike Jacobi preconditioning, the inversion in matrix formulation appears to rely on numerical calculation due to parameter variation depending on flow regimes, causing the method to be expensive. Note that the Jacobi preconditioning could use the analytical inversion method, i.e., an explicit form of the Navier–Stokes preconditioner can be utilized in numerical implementation.

The increase of the (1, 1) element in the Euler part of preconditioning has the additional benefit that it prevents the degeneration of the eigenvector system for small M. However, the attempt to modify the viscous Jacobian matrices in the Van Leer/Jacobi formulation was tried in order to avoid the null space in these matrices due to the absence of diffusion in the continuity equation, but it was not of much help because the corresponding element in the inverse Euler preconditioning is much stronger for $M \to 0$.

4. ANALYSIS OF VARIOUS PRECONDITIONING

Condition Number

Table I shows the condition number achieved by a variety of Navier–Stokes preconditioners in the three asymptotic regimes distinguished in Eq. (14). Only their 1D versions are considered, as a multidimensional analysis so far has not appeared possible.

For the original Navier–Stokes equations, the stiffness in the Euler limit is independent of *Re* and increases as the Mach number decreases; for viscosity-dominated flow, on the

other hand, it is independent of M, increasing when Re decreases. For acoustic-dominated viscous flow the stiffness varies with both M and Re. The use of preconditioning completely changes this pattern. The aim is to make the condition number equal to 1 or $\mathcal{O}(1)$; this has been achieved using Eqs. (13), (14) (but remember the growing mode), and there is hope that the Jacobi-type preconditioners can be improved up to this mark.

The listings in Table I are illustrated in detail by the four carpet plots, Figs. 13–18, based on numerically obtained eigenvalues. Figure 13 shows the condition number for the unpreconditioned 1D Navier–Stokes equations as a function of Mach number ($10^{-4} \leq M \leq 10^{-1}$) and cell-Reynolds number ($10^{-5} \leq Re \leq 10^{5}$). The number is seen to increase beyond bound for vanishing M or Re. Figure 14 shows that the Van Leer–Lee–Roe–Euler preconditioner creates a large usable domain, $Re \geq 1$, larger than the Euler domain. The same is true for Turkel's preconditioner, see Fig. 15. This explains results recently reported by Turkel *et al.* [14], *viz.* that the Euler preconditioner was effective in 2D and 3D viscous flow computations. The cell-Reynolds number in these calculations nowhere dropped below 1, not even in the most stretched boundary-layer cells.

Figures 16 and 18 show the improvements brought about by adding the Jacobi block to the Euler and Re-dependent forms of the Van Leer–Lee–Roe matrix. Finally, Figure 12 shows the condition number for just the Re-dependent Van Leer matrix: it is $\mathcal{O}(1)$ over the entire (M, Re) domain.

Linear Wave Propagation

Linear wave propagation analysis for an arbitrary system of viscous equations can be performed to analyze visually the convection and damping effect. Because the exact form of the time-dependent solution of viscous Burger's equation with cosine initial function is known, the transient solutions for a system may be obtained with proper linear superposition

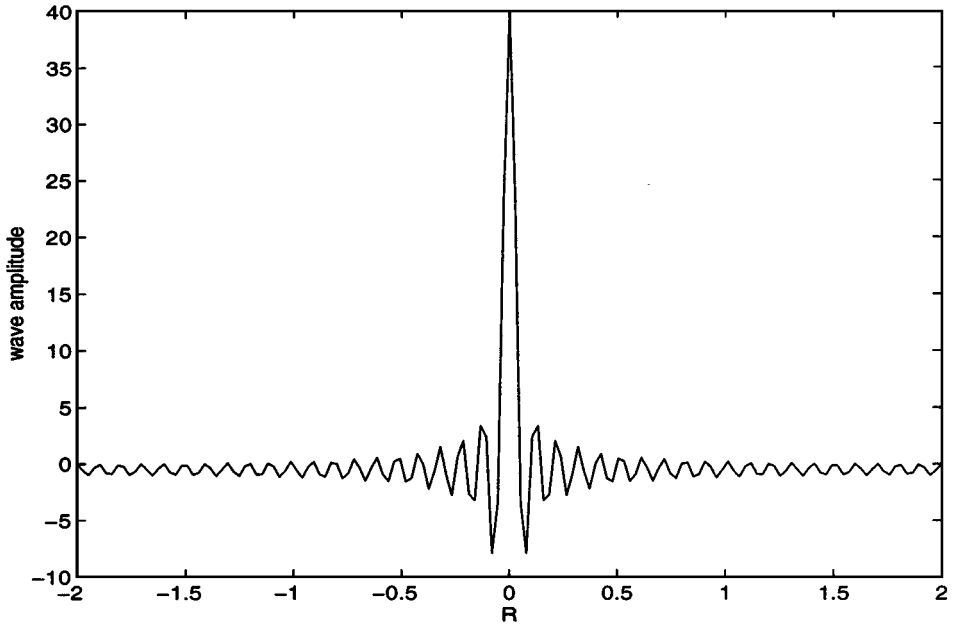

FIG. 7. Approximation of the Dirac Delta function by superposition of cosine functions up to 40 order.

of each frequency and sorting between each set of waves; this needs numerical calculation. The Delta function, purely composed with cosine functions, is used as an initial function; its wave forms will be easily obtained later at a certain time; 40 order of cosine functions is used for realization of the Delta function (see Fig. 7).

Figures 8–10 show how each preconditioner propagates the initial delta function, approximated by 40 cosines, with its own convection speed and damping rate. In all computations, the Mach number equals 0.1. From Fig. 8, the unpreconditioned case, we see the familiar feature of the inviscid limit that one of the waves moves slowly compared to the others, leading to a high condition number (11 for $M = 0.1$). For very low cell-Reynolds numbers,

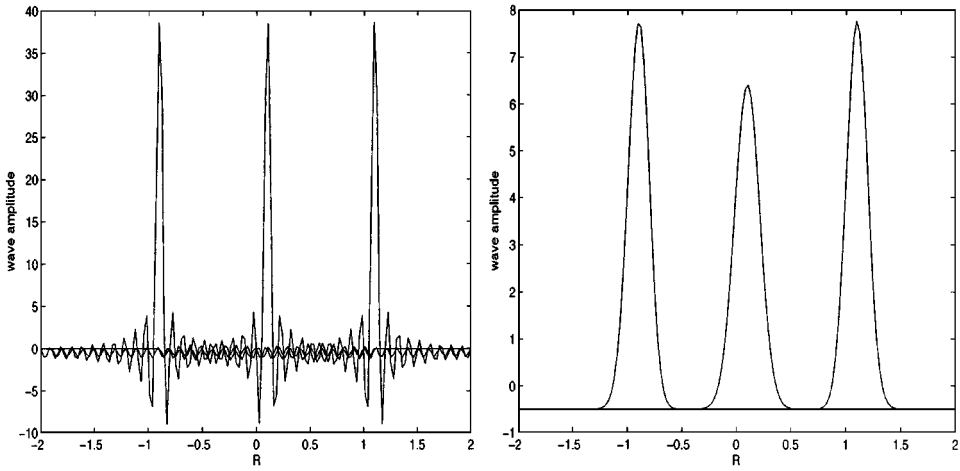

(a) $Re = 10^4$, $M = 0.1$, $K = 11$ (b) $Re = 1$, $M = 0.1$, $K = 7.7754$

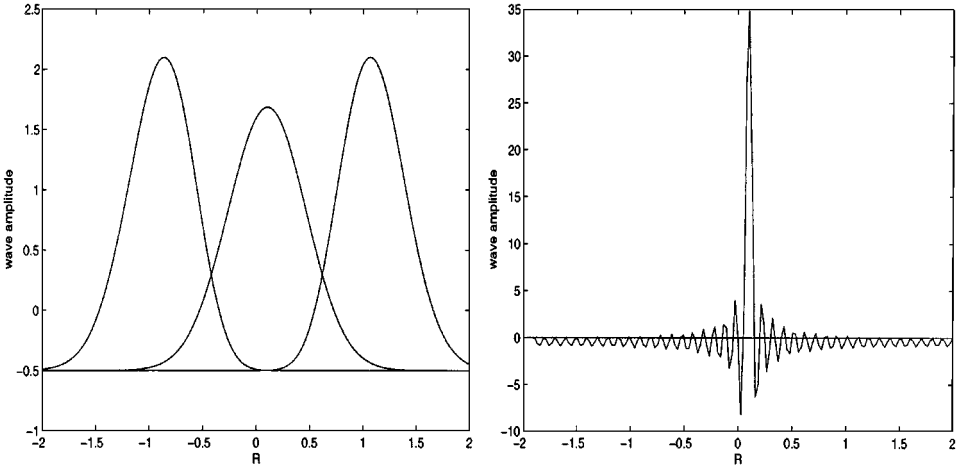

(c) $Re = 10^{-1}$, $M = 0.1$, $K = 1.3804$ (d) $Re = 10^{-3}$, $M = 0.1$, $K = 1863.9$

FIG. 8. Evolution of Delta functions: solution at $t = 1$ in the unpreconditioned case, for various Re_Δ; $M = 0.1$.

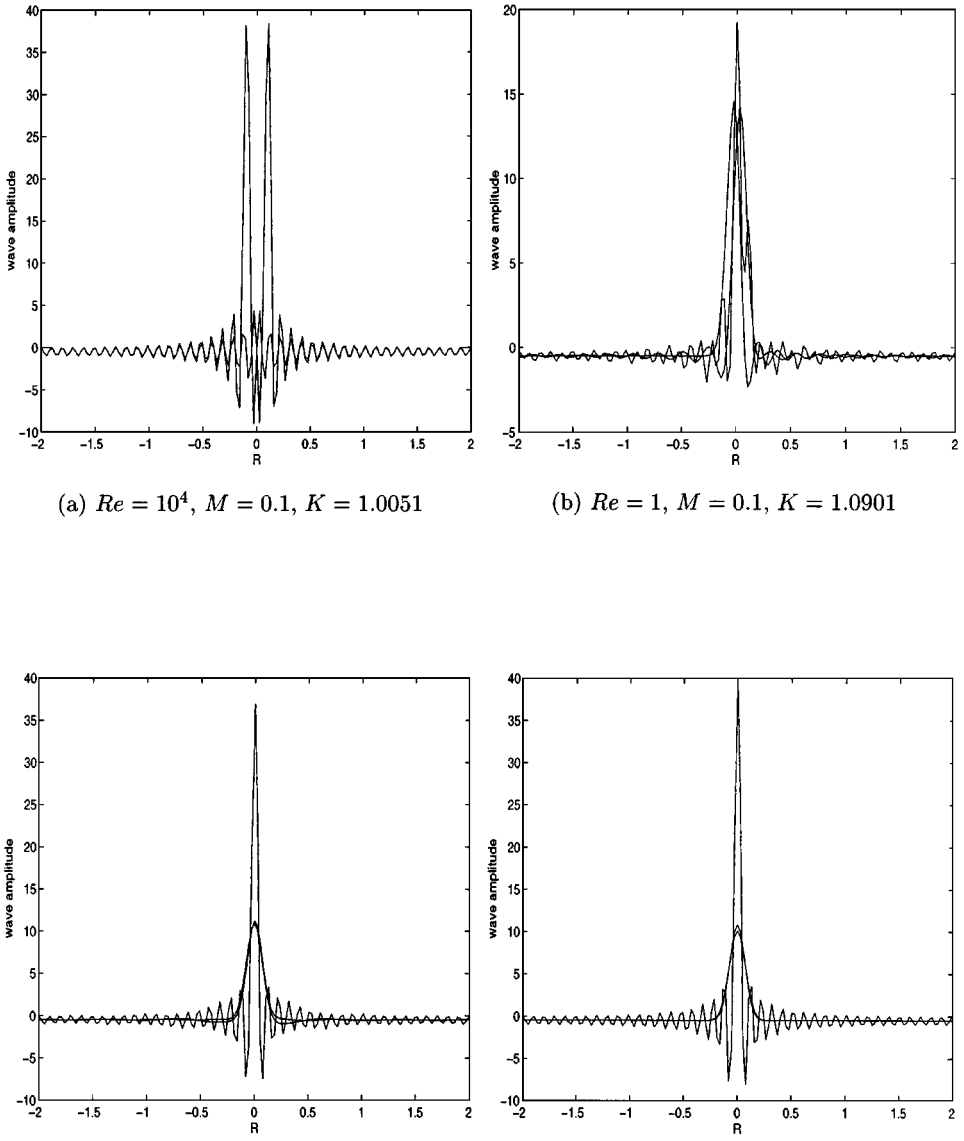

(a) $Re = 10^4$, $M = 0.1$, $K = 1.0051$

(b) $Re = 1$, $M = 0.1$, $K = 1.0901$

(c) $Re = 10^{-1}$, $M = 0.1$, $K = 12.7233$

(d) $Re = 10^{-3}$, $M = 0.1$, $K = 81.1495$

FIG. 9. Evolution of Delta functions: solution at $t = 1$ with Van Leer/Jacobi preconditioner.

one wave is undamped and moving slowly, but not very slowly, while the other waves have been fully damped out, leading to a huge condition number.

As can be seen from Fig. 9, the Van Leer/Jacobi Navier–Stokes preconditioner does a good job in reducing the condition number in the Euler limit (all propagation speeds equal in absolute value), but it suffers from a large condition number at very low cell-Reynolds numbers, due to an undamped stationary wave (the other stationary waves show significant damping). Figure 10 shows the improvement at very low cell-Reynolds numbers, after *Re*-dependence is put into the Euler part of the preconditioning. The undamped stationary wave starts to move, reducing the condition number, while the growing mode is absent.

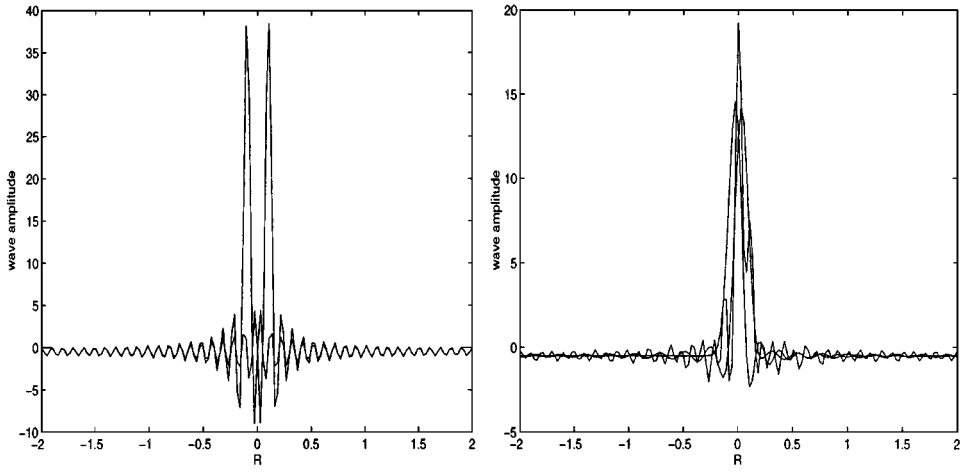

(a) $Re = 10^4$, $M = 0.1$, $K = 1.0051$ (b) $Re = 1$, $M = 0.1$, $K = 1.0901$

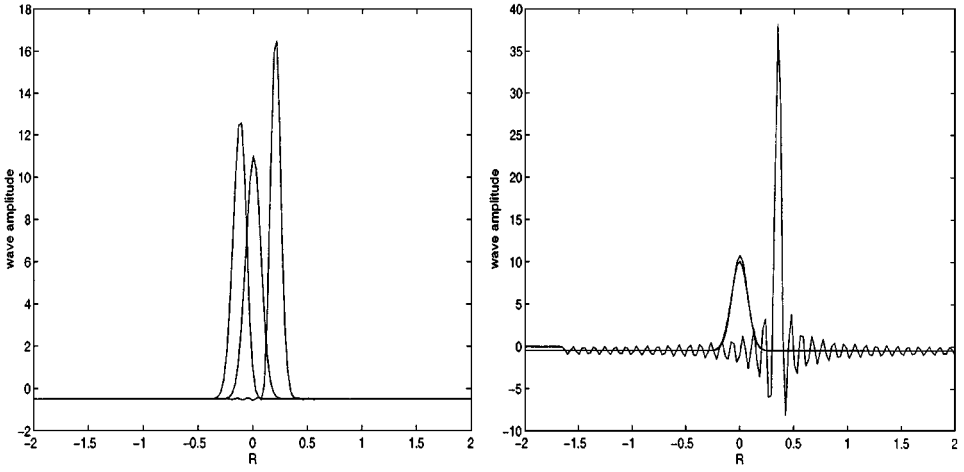

(c) $Re = 10^{-1}$, $M = 0.1$, $K = 5.0731$ (d) $Re = 10^{-3}$, $M = 0.1$, $K = 8.2390$

FIG. 10. Evolution of Delta functions: solution at $t = 1$ with *Re*-dependent Van Leer/Jacobi preconditioner.

5. NUMERICAL STUDIES

Below we give examples of the action of Navier–Stokes preconditioners.

First, consider initial values consisting of a uniform field with a pressure perturbation in one central cell. The Mach number of the background flow is low (0.1, 0.01); the flow angle is 0°. Table II shows the number of iterations needed for 5 orders of magnitude of residual reduction; the scheme is first-order upwind Euler with centrally differenced viscous terms, and single-stage time-stepping. The grid consists of 10×10 square cells. It is seen that the convergence by the preconditioned schemes is hardly influenced by the Mach or cell-Reynolds number, in contrast to the non-preconditioned scheme.

TABLE II

Number of Iterations Required for Reduction of the Density Residual by a Factor 10^{-5} (Unless a Smaller Exponent Is Indicated in Parentheses), in Calculating the Decay of a $10M^2$ % Pressure Perturbation in the Center of a Square Domain (10×10 Cells, $\mathcal{AR} = 1$)

	M					
	0.1			0.01		
Re_h	Unpc	VL/J	C/*Re*	Unpc	VL/J	C/*Re*
10^6	679	86	91	5183	86	91
10^4	679	86	92	5182	86	91
10^2	675	87	117	5100	87	116
1	1351	166	1830	5130	166	1858
10^{-2}	50000(−4.74)	194	133	5874	195	120
10^{-4}	50000(−2.79)	214	172	50000(−2.28)	214	121
10^{-6}	50000(−2.21)	214	170	50000(−2.21)	214	145

Note. Discrete Navier–Stokes operator (first-order upwind/central differencing) with single-stage time marching. Unpc = unpreconditioned; VL/J = Van Leer + Jacobi; C/*Re* = Chorin preconditioner modified to include *Re*-dependence.

The Van Leer/Jacobi and Chorin/*Re* preconditioners perform comparably, with some interesting differences. In the Euler limit the Van Leer matrix yields a lower condition number than the Chorin matrix (1 versus 2.6), explaining the somewhat faster convergence using the former. In the low-*Re* limit the situation is reversed, as the condition number for Van Leer/Jacobi is now a factor 5 larger than for Chorin/*Re*. For medium Reynolds number, $Re \approx 1$, the Chorin/*Re* matrix unexpectedly *slows down* convergence; this probably is the result of an inadequate choice of the switching function that connects the three branches of Eq. (14). It is clear that improvement is still possible here.

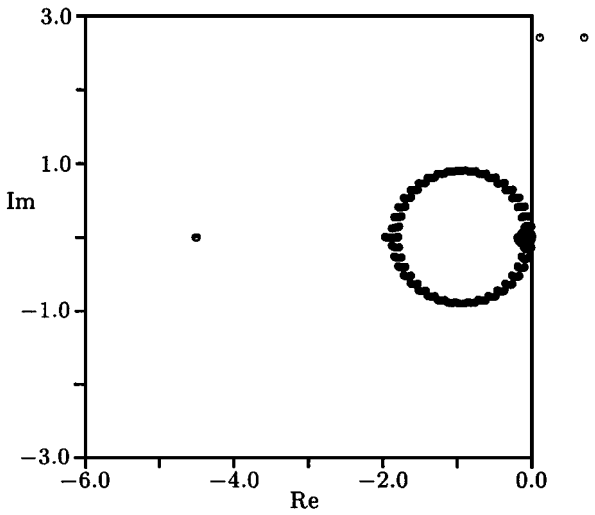

FIG. 11. Fourier footprint for unpreconditioned Navier–Stokes scheme (first-order upwind/central) with turbulence modeling. $M = 0.1$, $Re_h = 10^6$, $\frac{\|\mathbf{H_U}\|}{\nu} = 5 \times 10^8$, $\mathcal{AR} = 10$.

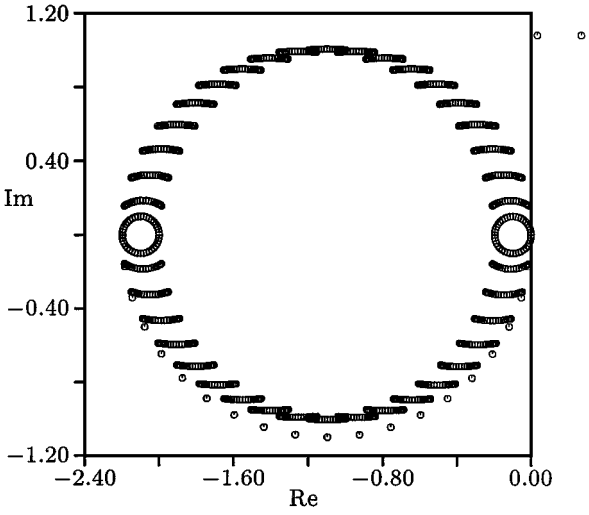

FIG. 12. Same as in Fig. 11, but after Van Leer/Jacobi preconditioning.

The second example is the computation of the development of a boundary layer on a flat plate ($M_\infty = 0.1$, $Re_L = 4 \times 10^4$). The cells right on the wall have an aspect ratio $\approx$1700. In this example, a Jacobi-type Navier–Stokes preconditioner is used. The analytical preconditioner is not valid for this model because this model contains a medium Reynolds number region which causes slow down convergence as can be seen from the first example. Figure 19 shows the steady flow field. As seen from the convergence histories in Fig. 20, convergence without preconditioning is slow to begin with and keeps slowing down, while the preconditioned scheme has no convergence problem at all.

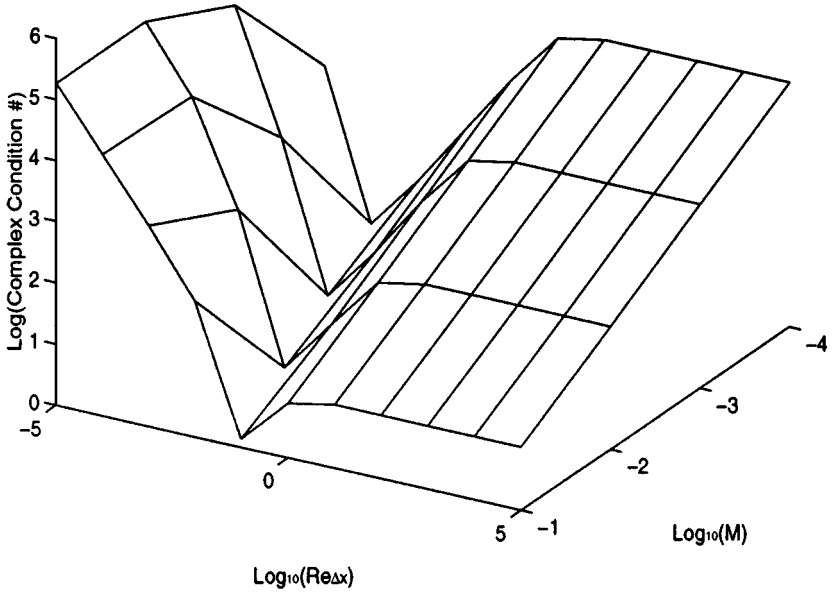

FIG. 13. Condition number for 1D Navier–Stokes equations without preconditioning.

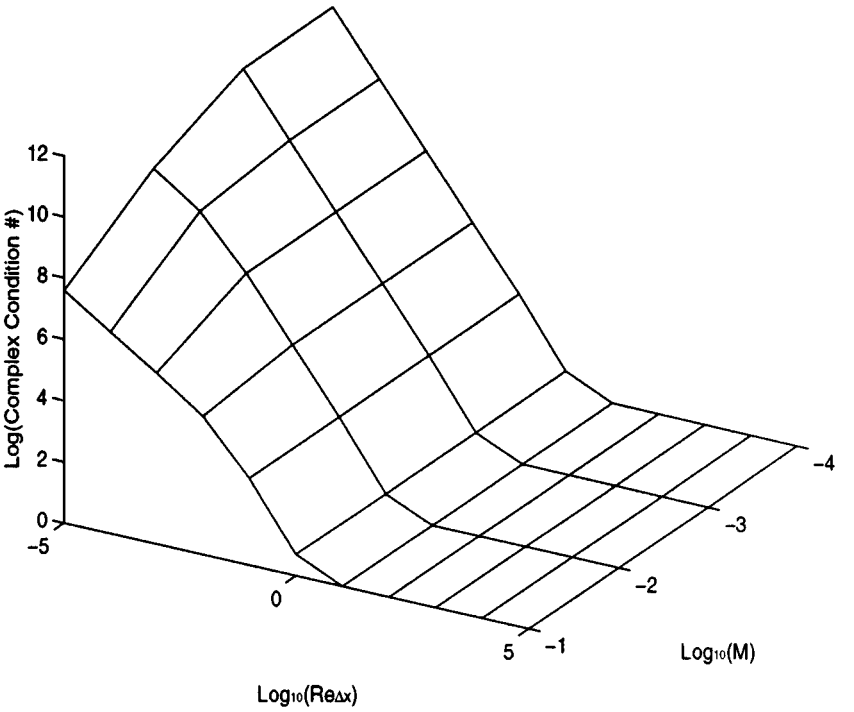

FIG. 14. Same as Fig. 13, using Van Leer's Euler preconditioner.

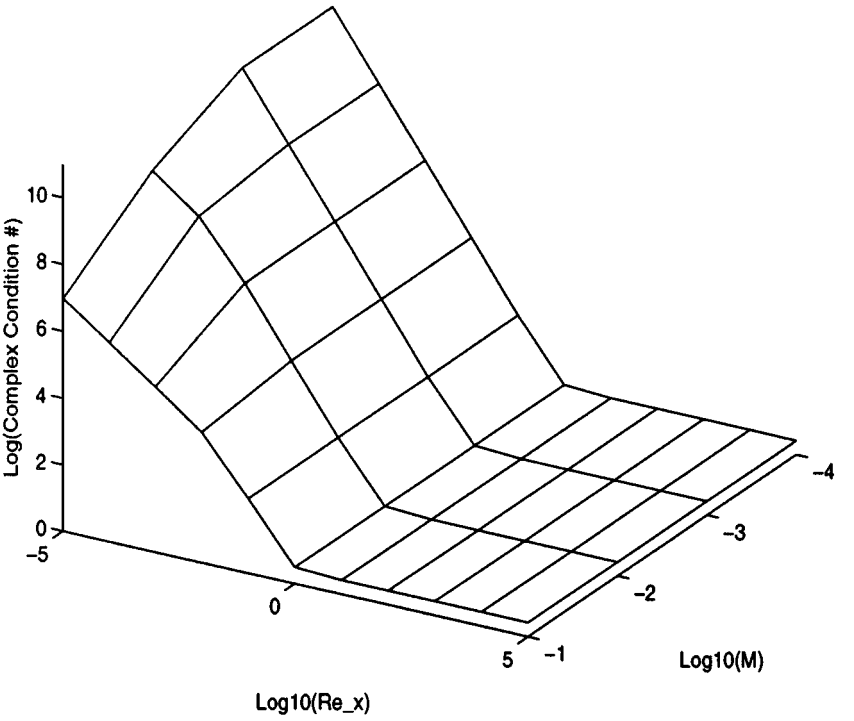

FIG. 15. Same as Fig. 13, using with Turkel's Euler preconditioner.

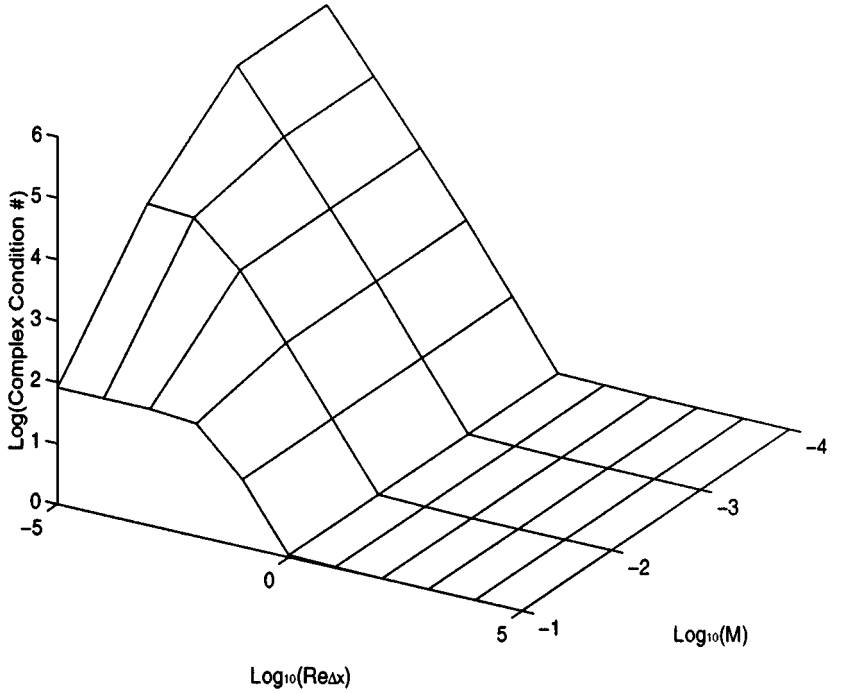

FIG. 16. Same as Fig. 13, using Van Leer/Jacobi preconditioning.

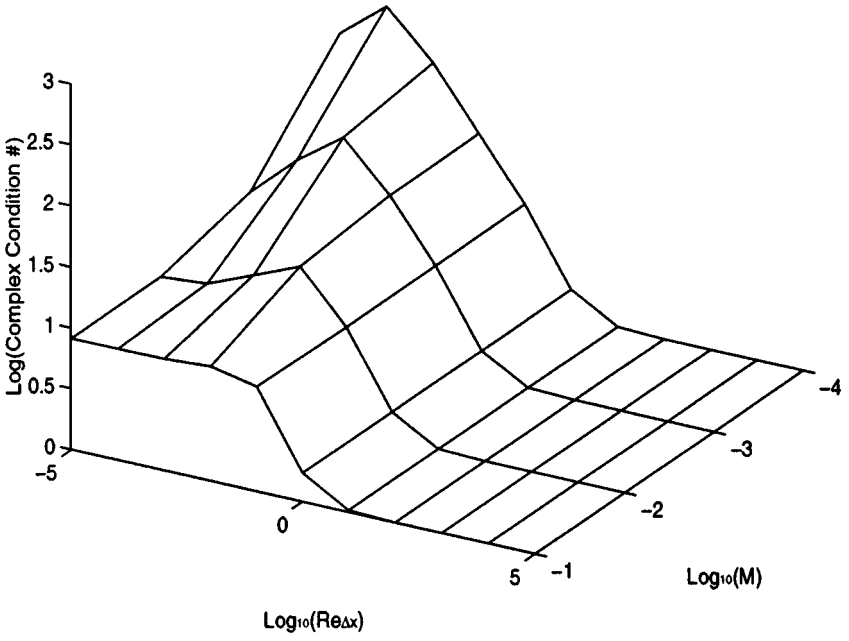

FIG. 17. Same as Fig. 13, using Van Leer's preconditioner modified to include *Re*-dependence, plus the viscous Jacobi block.

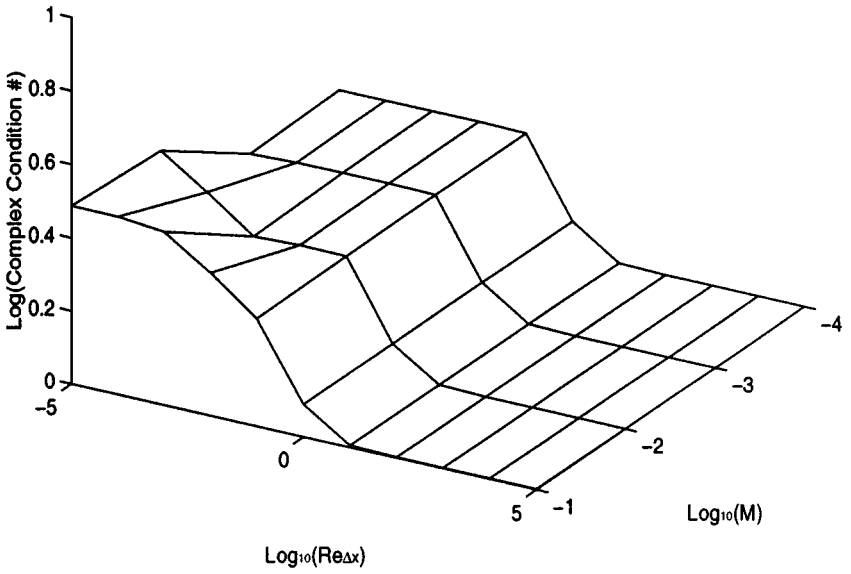

FIG. 18. Same as Fig. 13, using Van Leer's preconditioner modified to include *Re*-dependence.

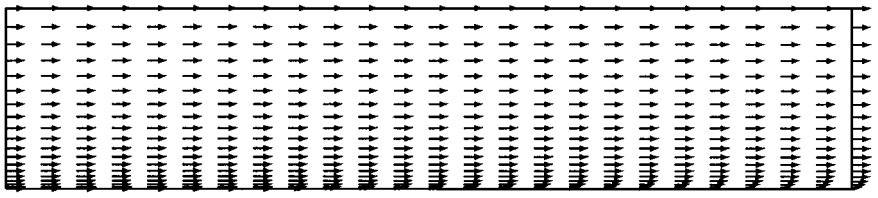

FIG. 19. Velocity field for boundary-layer development on a flat plate. $M = 0.1$, $Re_L = 4 \times 10^4$, 25×20 grid.

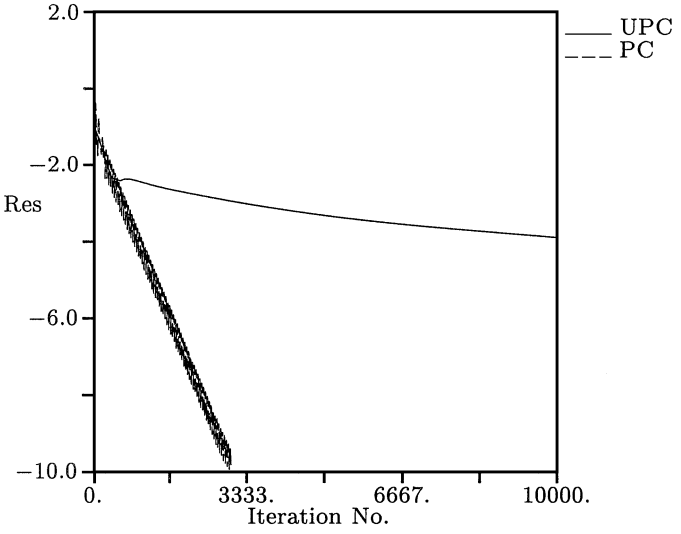

FIG. 20. Convergence histories for the flat-plate boundary-layer calculations. $M = 0.1$, $Re_L = 4 \times 10^4$, 25×20 grid. UPC = unpreconditioned, PC = Van Leer/Jacobi preconditioner.

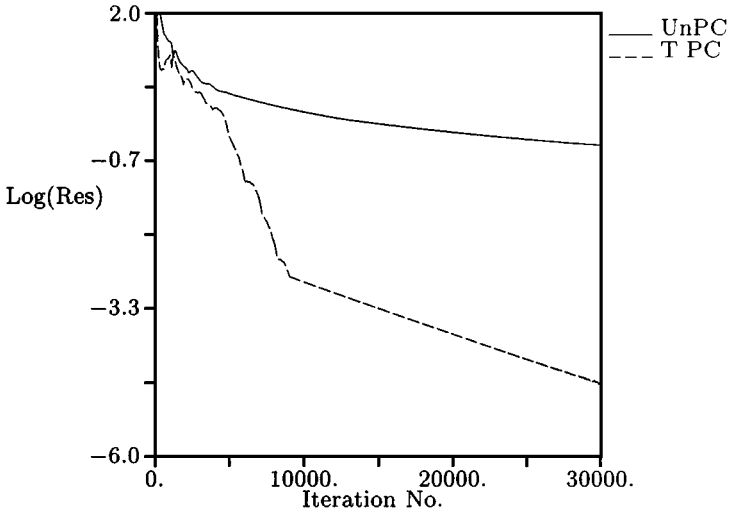

FIG. 21. Convergence histories for the flat-plate boundary-layer calculations with turbulence modeling. $M = 0.1$, $Re_L = 3 \times 10^5$, 25×50 grid. UnPC = unpreconditioned; T PC = Van Leer/Jacobi preconditioner including turbulent source-term Jacobian.

However, it has been known that even the Euler preconditioner may accelerate the viscous flow computation to some extent when the lowest local Reynolds number is not too low. Turkel's preconditioner already succeeded in computating the viscous flow with the Reynolds number up to around 1. But in this model, this is not the case: the cell-Reynolds number becomes much lower than 1 at some local cells in deep boundary layers. This means the Euler preconditioner cannot be used for acceleration of this viscous flow computation. A numerical test also shows that the Euler preconditioner produces a critical stability problem at a very low cell-Reynolds number, failing to compute this model problem. In this model, the large portion of convergence acceleration is believed to rely on the Euler preconditioning effect rather than the treatment of preconditioner for viscous effect because the computational domain with the Reynolds number higher than 1 is quite large. However, it is not possible to quantitively measure the effect of each Euler and viscous preconditioning due to the above-mentioned stability cause.

The third numerical test is the computation of the development of a *turbulent* boundary layer on the flat plate ($M_\infty = 0.1$, $Re_L = 3 \times 10^5$). The Spalart–Allmaras one-equation model is used for the turbulent transport. The convergence histories in Fig. 21 show that the Van Leer/Jacobi preconditioner of Eq. (12) indeed achieves convergence, overcoming the double stiffness due to the huge cell-aspect ratio ($\mathcal{AR} \approx 10^5$) and the large source term. Without preconditioning convergence is slow and eventually stalls.

6. CONCLUSIONS

The Navier–Stokes preconditioning is developed based on a Fourier analysis of the discretized equations and, following Venkateswaran and Merkle, a dispersion analysis of the differential equations. The principle of the Navier–Stokes preconditioning is to remove the dependence of the physical time scales on both the Mach number and the cell-Reynolds number. The discrete Fourier analysis suggests a "Jacobi-type" Navier–Stokes preconditioner, combining an optimal Euler preconditioner with the Jacobi block for the discretized

viscous/conductive terms. The dispersion analysis produces an analytical form of the preconditioner, which can equalize, in absolute value, the complex wave speeds of the Navier–Stokes equations; these include both effects of viscous damping and wave propagation.

The Jacobi-type Navier–Stokes preconditioner suffers from a large condition number due to one stationary non-damped wave at very low cell-Reynolds numbers. In contrast, the analytical *Re*-dependent Navier–Stokes preconditioner does not produce too large a condition number over the whole Reynolds-number range, but it suffers from a less-than-adequate switching function connecting the three asymptotic flow cases. In addition, for very low cell-Reynolds numbers ($Re \ll M^2$) the preconditioned equations obtain a growing mode, which must be stabilized, e.g., by implicit time-marching. If one insists on explicit *Re*-dependence, the combination with the viscous Jacobi block may overcome both obstacles of low cell-Reynolds numbers and large cell-aspect ratios. The modification of the embedded Euler preconditioner is restricted to putting *Re*-dependence into the (1, 1) element, which is easy to implement. This modification also helps to produce a less degenerated eigenvector structure at low Mach numbers, comparable to limiting the Mach number from below.

It should be explained that the very low *Re*-numbers where preconditioning may fail are mostly of academic interest. Our analysis shows that down to $Re_h \approx 1$ there is no need to deviate from a Euler preconditioner; this observation is supported by numerical evidence presented by other authors.

Numerical point-disturbance tests indicate that both types of preconditioners, Jacobi-type and analytical, can increase the convergence efficiency. However, when computing the development of a boundary-layer on a flat plate, the Jacobi-type preconditioner gives better convergence; this may be due to the automatic inclusion of the cell-aspect-ratio in the viscous Jacobi block.

REFERENCES

1. S. Abarbanel and D. Gottlieb, *Optimal Time Splitting for Two and Three Dimensional Navier–Stokes Equations with Mixed Derivatives*, ICASE Report 80-6, 1980.
2. S. R. Allmaras, *Analysis of Semi-implicit Preconditioners for Multigrid Solution of the 2-d Compressible Navier–Stokes Equations*, AIAA Paper 95-1651-CP, 1995.
3. P. Buelow, S. Venkateswaran, and C. L. Merkle, The effect of grid aspect ratio on convergence, in *AIAA 12th Computational Fluid Dynamics Conference, 1995*.
4. Y.-H. Choi and L. Merkle, The application of preconditioning in viscous flows, *J. Comput. Phys.* **105**, 207 (1993).
5. A. J. Chorin, A numerical method for solving incompressible viscous flow problems, *J. Comput. Phys.* **2** (1967).
6. A. G. Godfrey, *Topics on Spatially Accurate Methods and Preconditioning for the Navier–Stokes Equations with Finite-Rate Chemistry*, Ph.D. thesis, VPI & SU, 1992.
7. A. G. Godfrey, *Steps Towards a Robust Preconditioning*, AIAA Paper 94-0520, 1994.
8. A. G. Godfrey, R. W. Walters, and B. van Leer, *Preconditioning for the Navier–Stokes Equations with Finite-Rate Chemistry*, AIAA Paper 93-0535, 1993.
9. D. Lee, Design criteria for local euler preconditioning, *J. Comput. Phys.* **144**, 423 (1998).
10. D. Lee, *Local Preconditioning of the Euler and the Navier–Stokes Equations*, Ph.D. thesis, University of Michigan, 1996.
11. W.-T. Lee, *Local Preconditioning of the Euler Equations*, Ph.D. thesis, University of Michigan, 1991.
12. N. A. Pierce and M. B. Giles, *Preconditioning Compressible Flow Calculations on Stretched Meshes*, AIAA Paper 96-0889, 1996.

13. E. Turkel, Preconditioned methods for solving the incompressible and low speed compressible equations, *J. Comput. Phys.* **72** (1987).
14. E. Turkel, V. N. Vatsa, and R. Radespiel, *Preconditioning Methods for Low-Speed Flows*, AIAA Paper 96-2460-CP, 1996.
15. S. Venkateswaran and C. L. Merkle, Analysis of time-derivative preconditioning for the navier-stokes equations, in *6th International Symposium on Computational Fluid Dynamics, 1995*.